



# The reaction $NN \rightarrow NN\phi$

A.I. TITOVA<sup>a,b</sup>, B. KÄMPFER<sup>a</sup>, V.V. SHKLYAR<sup>b</sup>

<sup>a</sup>*Forschungszentrum Rossendorf, PF 510119, 01314 Dresden, Germany*

<sup>b</sup>*Bogoliubov Theoretical Laboratory, JINR Dubna, 141980 Dubna, Russia*

The sensitivity of polarization observables in the reaction  $NN \rightarrow NN\phi$  slightly above the threshold is studied with respect to the details of the one-boson exchange model and a possible admixture of hidden strangeness in the nucleon. It is shown that the finite-energy predictions differ strongly from the threshold predictions. A measurement of the beam - target asymmetry and the  $\phi$  decay anisotropy can help to disentangle the role of various reaction mechanisms.

*Key Words:* hadron reaction,  $\phi$  production, polarization observables

*PACS number(s):* 13.75.-n, 14.20.-c, 21.45.+v

## I. INTRODUCTION

The investigation of the reaction  $NN \rightarrow NN\phi$  is interesting for several reasons. First, the elementary total cross section [1] is an important input for the calculation of the  $\phi$  production in heavy-ion collisions [2]. In this case one might expect some change of the  $\phi$  width [3] due to the coupling to the decay channel  $\phi \rightarrow K^+ K^-$  and peculiarities according to the in-medium modification of the kaon properties [4,5]. Indeed, such measurements are under way with the  $4\pi$  detector FOPI at SIS in GSI/Darmstadt [6]. The electromagnetic decay channel  $\phi \rightarrow e^+ e^-$  will be investigated with the spectrometer HADES [7] also in GSI. A threshold-near measurement of the total cross section of the reaction  $pp \rightarrow pp\phi$  has been performed at SATURNE [8] and precision measurements of polarization observables are envisaged with the ANKE spectrometer at the cooler synchrotron COSY in Jülich [9].

Second, the  $\phi$  meson is thought to consist mainly of strange quarks, i.e.  $s\bar{s}$ , with a rather small contribution of the light  $u, d$  quarks. According to the OZI rule (cf. [10] for references) the  $\phi$  production should be suppressed if the entrance channel does not possess a considerable admixture of hidden or open strangeness. Indeed, the recent experiments on the proton annihilation at rest (cf. [10] for a compilation of data) point to a large apparent violation of the OZI rule, which is interpreted [10] as a hint to an intrinsic  $s\bar{s}$  component in the proton. However, the data can be explained by modified meson exchange models [11] without any strangeness content of nucleon or OZI rule violation. On the other hand the analysis of the  $\pi N$  sigma term [12] suggest that the proton might contain a strange quark admixture as large as 20%. Thus this issue remains rather controversial.

Therefore it is tempting to look for other observables [10,13] that are directly related to the strangeness content of the nucleon. In Ref. [14] it is shown that polarization observables of the  $\phi$  photoproduction are sensitive even to a small strangeness admixture in the proton. Other investigations concern the polarization observables in  $pp \rightarrow pp\phi$  reactions at the threshold [10,15]. It is found [15] that spin and parity conservation arguments result in a precise prediction for the beam - target asymmetry

$$C_{zz}^{BT} = \frac{d\sigma(S_i = 1) - d\sigma(S_i = 0)}{d\sigma(S_i = 1) + d\sigma(S_i = 0)} \quad (1)$$

for the  $pp \rightarrow pp\phi$  reaction at the threshold,  $C_{zz}^{BT} = 1$ , where  $S_i$  is the total spin in the entrance channel. It is further claimed [15] that the elements of the decay density matrix  $\rho_{rr'}$  (for notation see below) amount  $\rho_{00} = 0$ ,  $\rho_{\pm 1 \pm 1} = \frac{1}{2}$ . Real experiments, however, are performed at some finite energy above the threshold, and therefore the problem arises whether the threshold predictions are modified. More generally one should investigate the sensitivity of polarization observables to the strangeness admixture in the proton. An analysis of the threshold-near behavior of the unpolarized cross section is a necessary prerequisite, of course.

In the present work we employ a one-boson exchange (OBE) model to consider these mentioned issues. In Section II we present expressions for the kinematics, cross sections and spin density matrix. In Section III we describe our OBE approach. Section IV is devoted to parameter fixing. The threshold limit is analyzed in Section V. The results at finite energy above threshold are discussed in Section VI and summarized in Section VII.

## II. KINEMATICS AND OBSERVABLES

The corresponding cross section of  $\phi$  production in the reaction  $a + b \rightarrow c + d + \phi$ , where  $a, b$  and  $c, d$  label the incoming and outgoing nucleons (cf. Fig. 1), is related to the invariant amplitude  $T$  as

$$d\sigma = \frac{1}{2(2\pi)^5 \sqrt{s(s - 4M_N^2)}} |T|^2 \frac{d\mathbf{p}_c}{2E_c} \frac{d\mathbf{p}_d}{2E_d} \frac{d\mathbf{q}}{2E_\phi} \delta^{(4)}(P_i - P_f). \quad (2)$$

where  $p_n = (E_n, \mathbf{p}_n)$  with  $n = a, b, c, d$  and  $q = (E_\phi, \mathbf{q})$  are the four-momenta of the nucleons and the  $\phi$  meson in the center of mass system (c.m.s.), respectively. Hereafter  $\theta$  denotes the polar  $\phi$  meson angle,  $s = E_a + E_b$  is the total c.m.s. energy, and  $P_{i,f}$  is the total 4-momentum of the initial or final states. We use a coordinate system with  $\mathbf{z} \parallel \mathbf{p}_a$ ,  $\mathbf{y} \parallel \mathbf{p}_a \times \mathbf{q}$ . Among the five independent variables for describing the final state we choose  $E_\phi$ ,  $\Omega_\phi$  and  $\Omega_c$ . Then the energy  $E_c$  of particle  $c$  is defined by

$$E_c = \frac{AB \pm C\sqrt{B^2 - M_N^2(A^2 - C^2)}}{A^2 - C^2}, \quad (3)$$

with  $A = 2(\sqrt{s} - E_\phi)$ ,  $B = s - 2E_\phi\sqrt{s} + M_\phi^2$ ,  $C = 2q \cos \theta_{qp_c}$ , where  $\theta_{qp_c}$  is the angle between  $\mathbf{q}$  and  $\mathbf{p}_c$  determined by  $\cos \theta_{qp_c} = \cos \theta \cos \theta_c + \sin \theta \sin \theta_c \cos(\varphi - \varphi_c)$ ; the unindexed polar and azimuthal angles  $\theta$  and  $\phi$  belong to the vector  $\mathbf{q}$ . In calculations one has to use both solutions of Eq. (3) according to the considered kinematics. Finally, the fivefold differential cross section reads

$$\frac{d^5\sigma}{dE_\phi d\Omega_\phi d\Omega_c} = \frac{1}{8(2\pi)^5 \sqrt{s(s - 4M_N^2)}} |T|^2 \frac{qp_c^2}{|Ap_c + CE_c|}. \quad (4)$$

The total cross section is found by integration of over the available phase space.

One can consider the asymmetry Eq. (1) with integrated cross section or differential cross sections. In the general case the asymmetry depends also on  $E_\phi$ ,  $\Omega_\phi$  and  $\Omega_c$ .

We consider the decay angular distribution  $\mathcal{W}$  of the  $\phi$  meson in its helicity system where the  $\phi$  is at rest. The quantization axis  $\mathbf{z}'$  is chosen along the  $\phi$  meson velocity in the overall c.m.s., and the  $\mathbf{y}'$  axis is parallel to the vector  $\mathbf{p}_a \times \mathbf{q}$ . The decay angles  $\Theta, \Phi$  are defined as polar and azimuthal angles of the direction of flight of one of the decay particles in the  $\phi$  meson's rest frame. The decay angular distribution then reads

$$\frac{dN}{d \cos \Theta d\Phi} \equiv \mathcal{W}(\cos \Theta, \Phi) = \sum_{r,r'} M(r; \Theta, \Phi) \rho_{rr'} M^*(r'; \Theta, \Phi), \quad (5)$$

where  $M(r; \Theta, \Phi)$  is the decay amplitude,  $M(r; \Theta, \Phi) = M_0 d_{r, \lambda_\alpha - \lambda_\beta}^{1*}(\Phi, \Theta, -\Phi)$ , with  $r$  as the helicity of  $\phi$  meson;  $\lambda_{\alpha, \beta}$  denotes the helicity of decay particles and  $|M_0|^2$  is proportional to the decay width;  $D_{r,r'}^1$  stands for Wigner's rotation function. The angular distribution is normalized as

$$\int \mathcal{W}(\cos \Theta, \Phi) d\Omega = 1. \quad (6)$$

The density matrix  $\rho_{rr'}$  is expressed in terms of the production amplitudes  $T_\beta^r$

$$\rho_{rr'} = \frac{\sum_\beta T_\beta^r T_\beta^{r'*}}{\sum_{r,\beta} T_\beta^r T_\beta^{r*}}, \quad (7)$$

where  $\beta$  denotes a set of unobserved quantum numbers.

Assuming that in  $\phi \rightarrow K^+ K^-$  and  $\phi \rightarrow e^+ e^-$  decays  $\lambda_\alpha - \lambda_\beta = 0$  (i.e.  $\lambda_\alpha - \lambda_\beta = \pm 1$ ), and using the explicit form of the rotation function we get

$$\begin{aligned} \mathcal{W}^{K^+ K^-}(\cos \Theta, \Phi) &= \frac{3}{4\pi} \left[ \frac{1}{2} (\rho_{11} + \rho_{-1-1}) \sin^2 \Theta + \rho_{00} \cos^2 \Theta \right. \\ &\quad + \frac{1}{\sqrt{2}} (-\text{Re}\rho_{10} + \text{Re}\rho_{-10}) \sin 2\Theta \cos \Phi + \frac{1}{\sqrt{2}} (\text{Im}\rho_{10} + \text{Im}\rho_{-10}) \sin 2\Theta \sin \Phi \\ &\quad \left. - \text{Re}\rho_{1-1} \sin^2 \Theta \cos 2\Phi + \text{Im}\rho_{1-1} \sin^2 \Theta \sin 2\Phi \right], \end{aligned} \quad (8)$$

$$\begin{aligned} \mathcal{W}^{e^+ e^-}(\cos \Theta, \Phi) &= \frac{3}{8\pi} \left[ \frac{1}{2} (\rho_{11} + \rho_{-1-1}) (1 + \cos^2 \Theta) + \rho_{00} \sin^2 \Theta \right. \\ &\quad + \frac{1}{\sqrt{2}} (\text{Re}\rho_{10} - \text{Re}\rho_{-10}) \sin 2\Theta \cos \Phi - \frac{1}{\sqrt{2}} (\text{Im}\rho_{10} + \text{Im}\rho_{-10}) \sin 2\Theta \sin \Phi \\ &\quad \left. + \frac{1}{2} \text{Re}\rho_{1-1} \sin^2 \Theta \cos 2\Phi - \frac{1}{2} \text{Im}\rho_{1-1} \sin^2 \Theta \sin 2\Phi \right]. \end{aligned} \quad (9)$$

The decay distributions integrated over the azimuthal angle depend only on the diagonal matrix elements,

$$\begin{aligned} \mathcal{W}^{K^+ K^-}(\cos \Theta) &= \frac{3}{4} (1 - \rho_{00}) (1 + B^{K^+ K^-} \cos^2 \Theta), \\ \mathcal{W}^{e^+ e^-}(\cos \Theta) &= \frac{3}{8} (1 + \rho_{00}) (1 + B^{e^+ e^-} \cos^2 \Theta), \end{aligned} \quad (10)$$

where we use the normalization condition  $\rho_{11} + \rho_{-1-1} + \rho_{00} = 1$  and introduce the  $\phi$  decay anisotropies  $B$

$$\begin{aligned} B^{K^+K^-} &= -(1 - 3\rho_{00})/(1 - \rho_{00}), \\ B^{e^+e^-} &= (1 - 3\rho_{00})/(1 + \rho_{00}). \end{aligned} \quad (11)$$

### III. ONE-BOSON EXCHANGE MODEL

Similar to previous analyses of the bremsstrahlung in  $pp$  reactions [16] we use here the OBE model to parameterize the interaction in the reaction  $NN \rightarrow NN\phi$  by the set of relevant tree level diagrams with one meson exchange line. These reaction channels are depicted in Fig. 1. In diagram 1a the  $\phi$  is produced in an internal conversion in a  $\phi\rho\pi$  vertex, while diagram 1b is the contribution of the  $\phi$  "bremsstrahlung" due to a finite coupling of the  $\phi$  to the nucleon current, which might arise microscopically from the coupling of the  $\phi$  to the kaon cloud around the nucleon. Diagram 1c depicts a more exotic channel, namely the  $\phi$  shake-off reaction by the internal virtual meson flow analog to the  $\phi$  photoproduction [14,17]. It represents the emission from the vertex. (As alternative one could consider the  $s\bar{s}$  knock-out, but we assume here that the corresponding meson- $s\bar{s}$ - $\phi$  coupling constants are small.) Within the OBE model the diagrams 1a - c cover basically all reaction mechanisms. One expects that diagram 1a represents the dominating contribution to the OBE mechanism, and we call this process hereafter the conventional or pure OBE contribution.

#### A. Emission from internal meson line

This part of our OBE model is similar to the previously employed model [2]. The meson-nucleon and the  $\phi\rho\pi$  interaction Lagrangians read in obvious standard notation

$$\mathcal{L}_{MNN} = -ig_{\pi NN}\bar{N}\gamma_5\boldsymbol{\tau}\boldsymbol{\pi}N - g_{\rho NN}\left(\bar{N}\gamma_\mu\boldsymbol{\tau}N\boldsymbol{\rho}^\mu - \frac{\kappa_\rho}{2M_N}\bar{N}\sigma^{\mu\nu}\boldsymbol{\tau}N\partial_\nu\boldsymbol{\rho}_\mu\right), \quad (12)$$

$$\mathcal{L}_{\phi\rho\pi} = g_{\phi\rho\pi}\epsilon^{\mu\nu\alpha\beta}\partial_\mu\phi_\nu\text{Tr}(\partial_\alpha\rho_\beta\pi), \quad (13)$$

where  $\text{Tr}(\rho\pi) = \rho^0\pi^0 + \rho^+\pi^- + \rho^-\pi^+$ , and bold face letters denote isovectors. All coupling constants are dressed by monopole form factors  $F_i = (\Lambda_i^2 - m_i^2)/(\Lambda_i^2 - k_i^2)$ , where  $k_i$  is the four-momentum of the exchanged meson.

The total invariant amplitude is the sum of 4 amplitudes

$$T_\alpha^r = \sum_{m_c, d} \left( \xi_\alpha^1 T^r[ab; cd] + \xi_\alpha^2 T^r[ab; dc] + \xi_\alpha^3 T^r[ba; dc] + \xi_\alpha^4 T^r[ba; cd] \right) \quad (14)$$

with  $\xi_{pp}^1 = \xi_{pp}^3 = -\xi_{pp}^2 = -\xi_{pp}^4 = 1$ ,  $\xi_{pn}^1 = \xi_{pn}^3 = -1$ ,  $\xi_{pn}^2 = \xi_{pn}^4 = 2$ . The last two terms stem from the antisymmetrization or from charged meson exchange for  $pp$  or  $pn$  reactions, respectively. The first term in Eq. (14) for the  $pp$  reaction reads

$$T_{m_c m_d; m_a m_b}^r[ab; cd] = K(k_\pi^2, k_\rho^2) \Pi_{m_d m_b}(p_b, p_d) W_{m_c m_a}^r(p_a, p_c) \quad (15)$$

with

$$\begin{aligned}
K(k_\pi^2, k_\rho^2) &= \frac{g_{\pi NN} g_{\rho NN} g_{\phi \rho \pi}}{(k_\pi^2 - m_\pi^2)(k_\rho^2 - m_\rho^2)} \frac{\Lambda_\pi^2 - m_\pi^2}{\Lambda_\pi^2 - k_\pi^2} \frac{\Lambda_\rho^2 - m_\rho^2}{\Lambda_\rho^2 - k_\rho^2} \frac{\Lambda_{\phi \rho \pi}^{\rho^2} - m_\rho^2}{\Lambda_{\phi \rho \pi}^{\rho^2} - k_\rho^2} \frac{\Lambda_{\phi \rho \pi}^{\pi^2} - m_\pi^2}{\Lambda_{\phi \rho \pi}^{\pi^2} - k_\pi^2}, \\
\Pi_{m_d m_b}(p_b, p_d) &= \bar{u}(p_d, m_d) \gamma_5 u(p_b, m_b), \\
W_{m_c m_a}^r(p_a, p_c) &= i \epsilon_{\mu \nu \alpha \beta} k_\rho^\mu \Sigma_{m_c m_a}^\nu(k_\rho) q_\phi^\alpha \varepsilon^{*r, \beta}, \\
\Sigma_{m_c m_a}^\nu(k_\rho) &= \bar{u}(p_c, m_c) \left[ \gamma^\nu - i \frac{\kappa_\rho}{2M_N} \sigma^{\nu \nu'} k_{\rho \nu'} \right] u(p_a, m_a). \tag{16}
\end{aligned}$$

Here  $\varepsilon^{r, \beta}$  denotes the  $\phi$  polarization four-vector, and  $m_a \dots m_d$  are the nucleon spin projections on the quantization axis, and  $k_\rho = p_c - p_a$ ,  $k_\pi = p_b - p_d$ ;  $u$  stands for a Dirac bispinor. Detailed expressions of the functions  $\Pi$ ,  $W$  and  $\Sigma$  are displayed in the Appendix.

The amplitude in the  $\phi$  helicity frame is obtained from the amplitude in the c.m.s. by a standard Wigner rotation.

## B. Emission from external legs

The amplitude of direct  $\phi$  meson emission from the nucleon legs according to Fig. 1b is calculated similar to the real or virtual photon bremsstrahlung [18,19] in the few GeV region. The  $\phi NN$  vertex has the same structure as the  $\rho NN$  interaction (cf. second part of Eq. (12)), i.e., it possesses vector and tensor parts. Following Ref. [20] we use  $g_{\phi NN} = -0.24$  and  $\kappa_\phi = 0.2$ .

The internal zig-zag lines in Fig. 1b correspond to a suitably parameterized  $NN$  interaction in the form of the Born term of the OBE model with effective coupling constants and cut-off parameters and may be interpreted as effective  $\pi, \omega, \rho, \sigma$  meson exchanges. We would like to stress that this is an effective dynamical model which is appropriate in the few GeV region and which is different from the OBE model in the conventional sense. This model has been applied successfully to different reactions [18,19,16] and this encourages us to employ it for the  $\phi$  production too.

The total amplitude for the process 1b consists of  $4 \cdot 8$  contributions and has a similar structure as Eq. (14), where  $T[ab; cd]$  now reads

$$\begin{aligned}
T^r[ab; cd] &= -g_{\phi NN} \sum_{m=\pi, \sigma, \rho, \omega} (\bar{u}(p_c) [\Gamma^m \Omega_1^r + \Omega_2^r \Gamma^m] u(p_a)) [-i D^m] (\bar{u}(p_d) \Gamma^m u(p_b)), \\
\Omega_1^r &= \frac{\hat{p}_1 + M_N}{p_1^2 - M_N^2} \varepsilon_\mu^{*r} [\gamma_m u + i \frac{\kappa_\phi}{2M_N} \sigma^{\mu \nu} q_\nu], \quad \Omega_2^r = \varepsilon_\mu^{*r} [\gamma_\mu + i \frac{\kappa_\phi}{2M_N} \sigma^{\mu \nu} q_\nu] \frac{\hat{p}_2 + M_N}{p_2^2 - M_N^2}. \tag{17}
\end{aligned}$$

Here we use the notation  $p_1 = p_a - q$ ,  $p_2 = p_c + q$ , and  $\Gamma^m$  and  $D^m$  are effective coupling vertices and propagators of the two-body  $T$  matrix, respectively,

$$\begin{aligned}
D^{\pi/\sigma} &= \frac{i}{k^2 - m_{\pi/\sigma}^2}, \quad D_{\mu \nu}^{\rho/\omega} = -i \frac{g_{\mu \nu} - k_\mu k_\nu m_{\rho/\omega}^{-2}}{k^2 - m_{\rho/\omega}^2}, \\
\Gamma^\pi &= -ig_{\pi NN} \gamma_5, \quad \Gamma^\sigma = g_{\sigma NN}, \quad \Gamma_\mu^{\rho/\omega} = -g_{\rho/\omega NN} \left( \gamma_\mu + i \frac{\kappa_{\rho/\omega}}{2M_N} \sigma^{\mu \nu} k_\nu \right), \tag{18}
\end{aligned}$$

where  $k$  is the momentum of virtual meson and  $g_{mNN}$  is the corresponding coupling constant which is dressed by the above form factors. The explicit expression of the total amplitude is rather cumbersome and will not be displayed here. The most economic way to evaluate this amplitude is a direct numerical calculation of the Feynman diagrams including the spinor algebra. This method has been checked in a number of examples (including the OBE amplitude in Fig. 1a).

### C. Emission from vertex

The main ingredient of the  $\phi$  shake-off mechanism (cf. Fig. 1c) is the assumption that the constituent quark wave function of the proton contains, in addition to the usual  $uud$  component, a configuration with an explicit  $s\bar{s}$  contribution [17,21]. A simple realization of this picture is the following wave function in the Fock space [17]

$$|p\rangle = A|[uud]^{1/2}\rangle + B\left\{a_0|[uud]^{1/2} \otimes [s\bar{s}]^0]^{1/2}\rangle + a_1|[uud]^{1/2} \otimes [s\bar{s}]^1]^{1/2}\rangle\right\}, \quad (19)$$

where  $B^2$  denotes the strangeness admixture ( $|A|^2 + |B|^2 = 1$ ), and  $a_{0,1}^2 = \frac{1}{2}$  are the fractions of the  $s\bar{s}$  pair with spin 0 and 1. The superscripts represent the spin of each cluster, and  $\otimes$  indicates the vector addition of spins of the  $uud$  and  $s\bar{s}$  clusters and their relative orbital angular momentum ( $\ell = 1$ ). Details of the wave functions in the relativistic harmonic oscillator model can be found in [14]. Some estimates regarding the strangeness content in the nucleon advocate a few percent [10,13]. Otherwise, calculations based on the inclusion of extra kaonic degrees of freedom within a perturbative treatment give more than an order of magnitude smaller value of hidden strangeness [14,22] which is, however, likely to be dominated by nonperturbative effects [23]. That is the reason why we consider  $\phi$  bremsstrahlung and  $\phi$  shake-off independently.

We assume here as above that the exchanged effective mesons interact with the  $uud$  cluster as with a structureless particle and parameterize this interaction within the effective two-body  $T$  matrix. The  $s\bar{s}$  component is considered as spectator, that means only the configuration with spin  $S_{s\bar{s}} = 1$  is realized. The corresponding  $T$  matrix element is calculated in the rest frame of the splitting nucleon ( $p_a = (M_N, \mathbf{0})$ ) and it is expressed by

$$T_{m_c m_d; m_a m_b}^r [ab : cd]_{s.o.} = \sum_{m=\pi, \rho, \omega, \sigma} \sum_{m_x} M_{m_x; m_a}^{r N \rightarrow N\phi} T_{m_c m_d; m_x m_b}^{(m) NN \rightarrow NN}(p_c, p_d; p'_a, p_b) \quad (20)$$

with  $T^{(m) NN \rightarrow NN}$  as effective two-body  $T$  matrix

$$T_{m_c m_d; m_x m_b}^{(m) NN \rightarrow NN}(p_c, p_d; p'_a, p_b) = (\bar{u}(p_c, m_c) \Gamma^m u(p'_a m_x)) [-i D^m] (\bar{u}(p_d, m_d) \Gamma^m u(p_b, m_b)) \quad (21)$$

and with the vertices and propagators as in Eq. (18). The transition amplitude reads

$$M_{m_x; m_a}^{r N \rightarrow N\phi} = -i C_M \sqrt{\frac{3}{2}} \sum \left\langle 1m_\phi 1m \middle| jm_j \right\rangle \left\langle jm_j \frac{1}{2} m_x \middle| \frac{1}{2} m_a \right\rangle \hat{q}_m^L d_{m_\phi r}^1(\vartheta),$$

with

$$C_M = A^* B a_1 \frac{V(\mathbf{q}^L)}{\gamma_\phi \gamma_c^2}, \quad (22)$$

and  $p'_a = z p_a$ , where  $z \simeq 0.5$  is the momentum fraction carried by the  $uud$  cluster,  $\mathbf{q}^L$  denotes the  $\phi$  momentum in the laboratory system,  $\hat{q}_m^L$  is its projected unit vector in the circular basis, and  $V(\mathbf{k})$  stands for the wave function of the relative motion normalized as  $\int d\mathbf{k} V^2(\mathbf{k}) / ((2\pi)^3 2\sqrt{(\mathbf{k}^2 + M_\phi^2)}) = 1$ ;  $\gamma_{\phi,c}$  is the corresponding Lorentz factor which reflects the Lorentz contraction in the relativistic constituent model. In our calculations we use a Gaussian distribution  $V(x) = Nx \exp(-x^2/2\Omega)$  with  $\sqrt{\Omega} = 2.41 \text{ fm}^{-1}$  [14,17].

By making use of the numerical values of the Clebsch-Gordan coefficients we get the final expression for the amplitude  $M^{N \rightarrow N\phi}$  in the form

$$M_{m_x; m_a}^{rN \rightarrow N\Phi} = -i C_M \sqrt{\frac{1}{2}} \sum_{m_\phi=0,\pm 1} \left( \delta_{m_\phi 0} \left( -\hat{q}_z^L \delta_{m_a m_x} + (2m_a) \delta_{-m_a m_x} \hat{q}_\perp^L \frac{1}{\sqrt{2}} \right) \right. \\ \left. + \delta_{|m_\phi|1} \left( \hat{q}_z^L \delta_{-m_a m_x} \delta_{m_a m_\phi/2} + \delta_{m_a m_x} \hat{q}_\perp^L \left( \frac{m_\phi}{\sqrt{2}} - m_a \right) \right) \right) d_{m_\phi r}^1(\vartheta). \quad (23)$$

The two body scattering amplitude  $T_{m_c m_d; m_x m_b}^{(m) NN \rightarrow NN}$  for each exchange meson is found straightforwardly by using the functions  $\Pi$  and  $\Sigma$  in the Appendix. The final amplitude contains a sum over all exchanged mesons and consists of 2 direct and 2 exchange amplitudes for the  $pp$  reaction, and 2 direct and 0 ( $\omega, \sigma$ ) or 2 ( $\pi, \rho$ ) exchange amplitudes for the  $pn$  reaction to be taken with their proper isospin factors  $\xi_{pp(pn)}^m$  as in Eq. (14).

#### IV. FIXING PARAMETERS

The parameters of the two-body  $T$  matrix for  $\phi$  bremsstrahlung (Fig. 1b) and shake-off (Fig. 1c) are taken from Refs. [16,18] where quite reasonable agreement with data of different elastic and inelastic  $NN$  reactions is found.

The coupling constant  $g_{\phi\rho\pi}$  is determined by the  $\phi \rightarrow \rho\pi$  decay. The recent value  $\Gamma(\phi \rightarrow \rho\pi) = 0.69 \text{ MeV}$  results in  $g_{\phi\rho\pi} = 1.10 \text{ GeV}^{-1}$ . The remaining parameters of the OBE amplitude for the process 1a are taken from the Bonn model as listed in Table B.1 (Model II) of Ref. [24]. The cut-off parameter  $\Lambda_{\phi\rho\pi}^\rho = 2.9 \text{ GeV}$  is adjusted by a comparison of additional calculations including the channels discussed above and data [25] for the  $\pi^- p \rightarrow n\phi$  reaction. Note, that on this stage the result is not sensitive to the specific OBE model of the  $\pi p$  reaction, where  $\Lambda_{\phi\rho\pi}^\rho$  is used as fit parameter, that is, one can fit the data also with any other OBE model by using  $\Lambda_{\phi\rho\pi}^\rho$  as a free parameter. Turning to the  $pp$  reaction, however, we find that the cut-off  $\Lambda_{\phi\rho\pi}^\pi$  represents the main uncertainty of the model. It would be perfect to find it from the unpolarized cross section in this energy region and after that to study the polarization observables. Lacking precise data one has to use some reasonable guess which make our finite energy prediction rather qualitative estimates than exact predictions. However, as we show in the next section, some of the threshold prediction are "parameter independent". In any case, using our model one can easily refine our finite energy prediction when the needed data on unpolarized  $\phi$  production are available and fix  $\Lambda_{\phi\rho\pi}^\pi$ . The value  $\Lambda_{\phi\rho\pi}^\pi = 0.77 \text{ GeV}$  is provided by an analysis of the photoproduction of vector mesons [26],

and we use here this value having in mind, however, that the symmetry of the off-shell mesons in the  $\phi\rho\pi$  vertex would suggest  $\Lambda_{\phi\rho\pi}^\pi = \Lambda_{\phi\rho\pi}^\rho$  which can be employed as another reference value.

Note that the OBE model describes the data [25] in a limited region of  $\Delta_{\pi^-p\rightarrow n\phi} \equiv \sqrt{s} - M_N - M_\phi \leq 0.15$  GeV. At higher energies the OBE model overestimates the data. (In this region one could use an energy depending suppression factor at the vertices as in Ref. [1]).

Another type of uncertainty is related to the total phase ( $\eta = \exp(-i\delta)$ ) of the two-body  $T$  matrix. In the effective theory of Refs. [18,16] one fixes only the relative phase between different exchange amplitudes and, therefore, there are different possible solutions. The most natural one is the assumption that each exchange amplitude has the same phase as the pure amplitude of the process 1a, which is known. In this case the two-body  $T$  matrix must be real ( $\delta = 0$ ). In that instant we expect a strong interference between the radiation from the internal line and the external legs, because both amplitudes are almost real (at least in coplanar geometry), and a small interference with the radiation from the vertex, where the amplitude is almost imaginary. The opposite limit is based on the assumption that the unitary condition  $SS^+ = 1$  and the relation  $S = 1 - iT$  result in a forward scattering amplitude which is almost imaginary and negative. The assumption that the effective  $T$  matrix is responsible for the elastic forward scattering constrains the common phase, at least at small momentum transfer ( $\delta = \pi/2$ ). In this case one gets a strong interference between the OBE amplitude 1a and the radiation from vertex 1c, and a small one between these and the radiation from the legs 1b. The latter assumption is more reliable for high energy scattering, where the diffractive scattering (i.e. Pomeron exchange) is dominant; in near-threshold  $\phi$  production region it has rather a methodical interest. Nevertheless, for completeness we will consider both cases.

## V. THRESHOLD LIMIT

Let us now consider in some detail the threshold limit, where one can neglect terms proportional to  $|\mathbf{q}|/M_\phi$ ,  $|\mathbf{p}_{c,d}|/M_N$  in the amplitude. Spin observables in  $pp$  reaction are universal and do not depend on the specific model. So, for simplicity we first consider the OBE amplitude for the process 1a.

In the threshold limit the meson propagators and form factors become constants because they depend on the same variable  $k_{\rho,\pi}^2 \rightarrow k_0^2 = -M_N M_\phi$ , and using the explicit form of the functions  $\Pi$ ,  $\Sigma$  and  $W$  (cf. Appendix) we get

$$\begin{aligned} \Pi_{m_d m_b} &= \sqrt{M_N M_\Phi} (2m_b) \cos \theta_b \delta_{m_d m_b}, \\ \Sigma_{m_c m_a}^x &= (1 - \kappa_\rho) \sqrt{M_N M_\Phi} (2m_a) \cos \theta_a \delta_{-m_a m_c}, \\ \Sigma_{m_c m_a}^y &= i(1 - \kappa_\rho) \sqrt{M_N M_\Phi} \cos \theta_a \delta_{-m_a m_c} \\ W_{m_c m_a}^r &= \frac{1}{2} (1 - \kappa_\rho) M_\Phi^2 \sqrt{M_N (4M_N + M_\Phi)} \left\{ \varepsilon_x^{*r} + (2m_a) i \varepsilon_y^{*r} \right\} \delta_{-m_a m_c}. \end{aligned} \quad (24)$$

$\Sigma^{0,z}$  is not operative here, and one can express the amplitude in the simple form

$$T^r[ab;cd] = T_0 U^r[ab;cd]$$

with

$$\begin{aligned} T_0 &= (1 - \kappa_\rho) K(k_0^2) M_N M_\phi^{5/2} (M_N + \frac{1}{4} M_\phi)^{1/2}, \\ K(k_0^2) &= \frac{g_{\pi NN} g_{\rho NN} g_{\phi \rho \pi}}{(k_0^2 - m_\pi^2)(k_0^2 - m_\rho^2)} \frac{\Lambda_\pi^2 - m_\pi^2}{\Lambda_\pi^2 - k_0^2} \frac{\Lambda_\rho^2 - m_\rho^2}{\Lambda_\rho^2 - k_0^2} \frac{\Lambda_{\phi \rho \pi}^{\rho^2} - m_\rho^2}{\Lambda_{\phi \rho \pi}^{\rho^2} - k_0^2} \frac{\Lambda_{\phi \rho \pi}^{\pi^2} - m_\pi^2}{\Lambda_{\phi \rho \pi}^{\pi^2} - k_0^2}, \\ U^r[ab;cd] &= -4 \sqrt{2} m_a m_b \cos \theta_b \delta_{-m_a m_c} \delta_{m_b m_d} d_{2m_a r}^1(\theta). \end{aligned} \quad (25)$$

The spin is transferred to the  $\phi$  meson only in the  $NN\rho$  vertex by a nucleon spin-flip, and for  $T^{\pm 1}(\theta = 0) \neq 0$  only for  $m_a = \pm \frac{1}{2}$ . Summation of  $|T^r|^2$  over the spin projections  $m_{c,d}$  of the outgoing particles leads to

$$\sum_{m_{c,d}} |T_\alpha^r|^2 = 2 T_0^2 \Delta_{m_a m_b}^\alpha |d_{2m_a r}^1(\theta)|^2, \quad (26)$$

where  $\Delta_{m_a m_b}^{pp} = 8 \delta_{m_a m_b}$ , and  $\Delta_{m_a m_b}^{pn} = 2(1 + 8 \delta_{m_a m_b})$ . Using these equations we get the threshold limits for the beam - target asymmetry  $C_{zz}^{BT} = 1$  for  $pp$  collisions. The diagonal spin density matrix elements are  $\rho_{00}^{\text{thr}} = \frac{1}{2} \sin^2 \theta$  and  $\rho_{\pm 1 \pm 1}^{\text{thr}} = \frac{1}{2}(1 + \cos^2 \theta)$ . Note that, as we mentioned above for the  $pp$  reaction, this predictions are universal because they reflect spin and parity conservation for two identical fermions and do not depend on the specific mechanism. All of the above discussed amplitudes are satisfy the same relations.

For the  $pn$  reaction this kind of predictions depend on the model and generally on model parameters, say, on the relative contribution of neutral and charged meson exchange to the two-body  $T$  matrix in  $\phi$  bremsstrahlung, shake-off and others. However, for the OBE amplitude 1a the threshold predictions for the beam-target asymmetry and spin-density matrix are parameter independent. From Eq. (26) we get for the beam-target asymmetry  $C_{zz}^{BT} = 0.8$ , which means that the ratio of singlet to triplet spin states is  $\frac{1}{9}$ . The diagonal spin density matrix elements are the same as in the  $pp$  reaction.

Using Eq. (26) we can make an important prediction: the ratio of the unpolarized cross sections in  $pn$  and  $pp$  reactions is  $\sigma_{np}/\sigma_{pp} = 5/2 \cdot \frac{1}{2} = 5$ , where the factor  $\frac{1}{2}$  in the  $pp$  cross section represents the symmetry factor. This prediction does not depend on the OBE model parameters. As we shall see below, the OBE amplitude 1a dominates, hence fore we can expect that the ratio of the corresponding total cross sections would be close to the factor 5.

## VI. RESULTS

Our results for the total cross section of the  $pp$  reaction are shown in Fig. 2 by the solid lines. As we mentioned above, the comparison of the momenta at the  $\pi\rho\phi$  vertex in the  $NN \rightarrow NN\phi$  reaction with the  $\pi N \rightarrow N\phi$  reaction shows a limited reliability of the pure OBE model to the region of  $\Delta_s \equiv \sqrt{s} - 2M_N - M_\phi \leq 0.15$  GeV. One can easily extend the model to a wider energy region, say  $\Delta_s \sim 1$  GeV, by reducing the cross section with

the effective cut-off factor  $\propto \exp(-0.8 \Delta_s)$  resulting from the energy depending coupling strengths in Ref. [16]. The resulting cross section is shown by the dashed lines.

Triangles in Fig. 2 show our prediction for the  $\phi$  bremsstrahlung contribution 1b. Open and full circles show the predictions for the shake-off channel 1c with a strangeness probabilities  $B^2 = 0.01$  and  $0.05$ , respectively. The dot-dashed lines show the contributions from the pure OBE channel 1a. The  $\phi$  bremsstrahlung and shake-off contributions have the same order of magnitude. The shake-off channel in this reaction is reduced strongly by the form factor  $V$  in Eq. (22). The solid lines show the coherent sum of all amplitudes with  $B^2 = 0.05$ . The left (right) panel in Fig. 2 displays the result for a purely real (imaginary) phase of the two-body  $T$  matrix. The interference between the pure OBE amplitude 1a and the shake-off amplitude 1c in the first case is rather small and therefore the difference between the results of the shake off with  $a_1 = \pm 1$  is not seen. But it may be seen, in principle, in second case, where the positive value of  $a_1$  is marked by crosses. In spite of the difference between the separate contributions of the conventional OBE channel 1a and the exotic  $\phi$  production channels, which is more than an order of magnitude at  $\Delta_s \simeq 0.1$  GeV for the above given parameters and  $g_{\phi NN} \simeq -0.24$  and  $B^2 \leq 0.05$ , the interference may amount up to 50% of the total cross section.

The cross section for the  $pn$  reaction is greater by a factor  $\simeq 5$  as given already in our threshold-near prediction.

The interference between the conventional OBE process 1a and the other exotic  $\phi$  channels 1b,c is much stronger in polarization observables. Fig. 3 shows our finite-energy predictions for the beam - target asymmetry Eq. (1) as a function of the  $\phi$  production angle  $\theta$  at fixed recoil nucleon angles  $\theta_{p'}, \varphi_{p'} = \pi$  at  $\Delta_s = 0.1$  GeV and  $|\mathbf{q}| = \frac{2}{3}\lambda(s, M_\phi^2, 4M_N^2)/(2\sqrt{s})$  for the  $pp$  reaction for separate channels ( $\lambda$  is the usual triangle function). The contribution from the OBE channel 1a is depicted by the dot-dashed line, while the  $\phi$  bremsstrahlung contribution 1b is marked by triangles, and the  $\phi$  shake-off process 1c is marked by dots. The threshold prediction is the dashed line.

One can see that the asymmetry for the conventional OBE channel 1a and the  $\phi$  bremsstrahlung channel 1b are qualitatively very similar. But in the case of a real phase of the two-body  $T$  matrix there is a strong "destructive" interference in the asymmetry which forces a significant decrease of the total asymmetry. This is shown in Fig. 4 (left panel) where we display the beam - target asymmetry as a coherent sum of all channels. Solid, dotted and dash-dotted lines correspond to  $B^2 = 0, 0.01$  and  $0.05$ , respectively. The contribution from the shake-off process is rather small. The strong decrease of the total asymmetry may be considered even as interesting quantitative manifestation of the  $\phi$  bremsstrahlung process 1b. If one would use instead of  $g_{\phi NN} = -0.24$  the same positive quantity, then the asymmetry results in much larger values  $0.4 \dots 0.6$ ; the corresponding result is marked by crosses.

The right panel of Fig. 4 illustrates the asymmetry for a purely imaginary two-body  $T$  matrix. The crosses mark a positive value of  $a_1$  in Eq. (19). The sign of  $a_1$  is still unknown. The area between marked and unmarked dot-dashed lines represents the theoretical uncertainty of the predictions for  $B^2 = 0 \dots 0.05$ . For positive values of  $a_1$  the asymmetry differs noticeably from the pure OBE process 1a prediction and may reach even negative values.

The influence of this uncertainty is smaller for the spin density matrix Eq. (7). Fig. 5 (left panel, same notation as in Fig. 3) depicts  $\rho_{00}$  separately for each channel at  $\Delta_s = 0.1$

GeV. The anisotropy of the angular distribution in 2-body decays  $\phi \rightarrow a^+a^-$  is given by Eqs. (10,11). One can see in Fig. 5 (right panel, same notation as in right panel of Fig. 4) a strong modification of the anisotropy for  $\phi \rightarrow e^+e^-$  decays by the shake-off mechanism at small angles  $\theta$ . This effect is smaller for  $K^+K^-$  decays. The dotted and dot-dashed lines marked by diamonds correspond to calculations with real two-body  $T$  matrix and  $B^2=0.01$  and 0.05, respectively.

In  $pn$  reactions all these polarization effects exist too, but they are not so strong as in the  $pp$  reactions. That is because the OBE channel 1a here is a factor of 5 greater, while the contribution of the "exotic" channels remains on the same level as in the  $pp$  case.

Finally, we would like to mention that the choice  $\Lambda_{\phi\phi\pi}^\pi = 2.9$  GeV (instead of 0.77 GeV) increases the OBE contribution 1a by factor  $4 \cdots 6$ , while the other "exotic" contributions remain on the same level. This results in a decrease of their relative role in polarization observables which then become much closer to the pure OBE channel 1a predictions.

## VII. SUMMARY

In summary we calculate within an extended OBE model with "exotic"  $\phi$  production channels the cross section and polarization observables for the reaction  $NN \rightarrow NN\phi$ . We predict the threshold behavior of cross sections for polarized and unpolarized reactions. Above the threshold the polarization observables differ strongly from the threshold predictions and behave differently for each channel. This means that measurements of the beam - target asymmetry and anisotropy of the  $\phi$  decays may reveal the presence of hidden strangeness and help disentangling various reaction mechanisms.

**Acknowledgments:** Useful discussions with C.M. Ko, U. Mosel, A.A. Sibirtsev and members of the DISTO collaboration are gratefully acknowledged. One of the authors (A.I.T.) acknowledges the warm hospitality of the nuclear theory group in the Research Center Rossendorf. This work is supported by the BMBF grant 06DR829/1 and the Heisenberg-Landau program.

## APPENDIX A: FUNCTIONS $\Pi, \Sigma$ AND $W$ FOR THE OBE AMPLITUDE

$\Pi_{m_d m_b}(p_b, p_d)$ :

Using the definition of the Dirac spinor

$$u(p) = \sqrt{E_p + M} \begin{pmatrix} 1 \\ \alpha \boldsymbol{\sigma} \cdot \mathbf{n} \end{pmatrix} \chi(m_p), \quad \alpha \equiv \sqrt{\frac{E_p - M_N}{E_p + M_N}}, \quad (\text{A1})$$

and the identity

$$\chi_f^+ (\boldsymbol{\sigma} \cdot \mathbf{A}) \chi_i = 2m_i A_z \delta_{m_i m_f} + (A_x + 2im_i A_y) \delta_{m_i - m_f}, \quad (\text{A2})$$

we find

$$\begin{aligned} \Pi_{m_d m_b} = C_{bd} & [ 2m_d (\alpha_b \cos \theta_b - \alpha_d \cos \theta_d) \delta_{m_b m_d} \\ & - \alpha_d \sin \theta_d \exp(-2im_d \varphi_d) \delta_{m_b - m_d} ], \end{aligned} \quad (\text{A3})$$

where  $C_{bd} = \sqrt{(E_b + M_N)(E_d + M_N)}$ . When the incoming particle moves along the  $z$  axis,  $\cos \theta_b = \pm 1$ .

$\Sigma_{m_c m_a}^\nu(k_\rho)$ :

Calculating  $\Sigma^\nu(k_\rho)$ , where  $k_\rho = p_c - p_a$ , we use Gordon's identity

$$\bar{u}(p_c) [\gamma^\nu] u(p_a) = \frac{1}{2M} \bar{u}(p_c) \left[ (p_a + p_c)^\nu + i\sigma^{\nu\nu'} k_{\rho\nu'} \right] u(p_a). \quad (\text{A4})$$

which allows to express  $\Sigma^\nu$  as the sum

$$\begin{aligned} \Sigma_{m_c m_a}^\nu &= \Sigma_{1 m_c m_a}^\nu + \Sigma_{2 m_c m_a}^\nu, \\ \Sigma_{1 m_c m_a}^\nu &= \frac{\kappa_\rho}{2M_N} P_{ac}^\nu \bar{u}(p_c) u(p_a), \\ \Sigma_{2 m_c m_a}^\nu &= (1 - \kappa_\rho) \bar{u}(p_c) \gamma^\nu u(p_a) \end{aligned} \quad (\text{A5})$$

with  $P_{ac} = p_a + p_c$ . Direct evaluation of  $\Sigma_1$  gives

$$\begin{aligned} \Sigma_{1 m_c m_a}^\nu &= \frac{\kappa_\rho}{2M_N} P_{ac}^\nu C_{ac} [(1 - \alpha_a \alpha_c \cos \theta_a \cos \theta_c) \delta_{m_a m_c} \\ &\quad - 2m_a \alpha_a \alpha_c \cos \theta_a \sin \theta_c \exp(-2im_c \varphi_c) \delta_{m_a - m_c}]. \end{aligned} \quad (\text{A6})$$

Explicit expressions for the components of  $\Sigma_2^\nu$  read

$$\begin{aligned} \Sigma_{2 ac}^0 &= (1 - \kappa_\rho) C_{ac} [(1 + \alpha_a \alpha_c \cos \theta_a \cos \theta_c) \delta_{m_a m_c} \\ &\quad + 2m_a \alpha_a \alpha_c \cos \theta_a \sin \theta_c \exp(-2im_c \varphi_c) \delta_{m_a - m_c}], \end{aligned} \quad (\text{A7})$$

$$\begin{aligned} \Sigma_{2 ac}^x &= (1 - \kappa_\rho) C_{ac} [\alpha_c \sin \theta_c \exp(-2im_c \varphi_c) \delta_{m_a m_c} \\ &\quad + 2m_a (\alpha_a \cos \theta_a - \alpha_c \cos \theta_c) \delta_{m_a - m_c}], \end{aligned} \quad (\text{A8})$$

$$\begin{aligned} \Sigma_{2 ac}^y &= i(1 - \kappa_\rho) C_{ac} [2m_a \alpha_c \sin \theta_c \exp(2im_c \varphi_c) \delta_{m_a m_c} \\ &\quad + (\alpha_a \cos \theta_a - \alpha_c \cos \theta_c) \delta_{m_a - m_c}], \end{aligned} \quad (\text{A9})$$

$$\begin{aligned} \Sigma_{2 ac}^z &= (1 - \kappa_\rho) C_{ac} [(\alpha_a \cos \theta_a + \alpha_c \cos \theta_c) \delta_{m_a m_c} \\ &\quad + 2m_a \alpha_c \sin \theta_c \exp(-2im_c \varphi_c) \delta_{m_a - m_c}]. \end{aligned} \quad (\text{A10})$$

$W_{ac}^r(p_a, p_c)$ :

For calculating  $W^r$  we use the identity

$$\begin{aligned} \epsilon_{\mu\nu\alpha\beta} k_\rho^\mu \Sigma^\nu q_\phi^\alpha \varepsilon^{*r,\beta} &= k_{\rho 0} \mathbf{q} \cdot (\boldsymbol{\Sigma} \times \boldsymbol{\varepsilon}^{*r}) - q_0 \mathbf{k}_\rho \cdot (\boldsymbol{\Sigma} \times \boldsymbol{\varepsilon}^{*r}) \\ &\quad + \Sigma_0 \boldsymbol{\varepsilon}^{*r} \cdot (\mathbf{k}_\rho \times \mathbf{q}) - \varepsilon_0^{*r} \boldsymbol{\Sigma} \cdot (\mathbf{k}_\rho \times \mathbf{q}), \end{aligned} \quad (\text{A11})$$

which allows to express amplitude  $W^r$  in compact form as

$$W^r = i (\mathbf{A} \cdot \mathbf{C}^r + \mathbf{B} \cdot \mathbf{D}^r), \quad (\text{A12})$$

where

$$\begin{aligned} \mathbf{A} &= k_{\rho 0} \mathbf{q} - q_0 \mathbf{k}_\rho, \quad \mathbf{B} = \mathbf{k}_\rho \times \mathbf{q}, \\ \mathbf{C}^r &= \boldsymbol{\Sigma} \times \boldsymbol{\varepsilon}^{*r} \quad \mathbf{D}^r = \Sigma_0 \boldsymbol{\varepsilon}^{*r} - \varepsilon_0^{*r} \boldsymbol{\Sigma}. \end{aligned} \quad (\text{A13})$$

(for simplicity we skip here the arguments  $p_a, p_c, \dots$  in  $W^r$  and  $\Sigma^r$ ). The independent  $\phi$  meson polarization vectors  $\varepsilon^r = (\varepsilon_x^r, \varepsilon_y^r, \varepsilon_z^r, \varepsilon_0^r)$  with  $r = 1, 2, 3$ , read

$$\begin{aligned}\varepsilon^1 &= (\cos \theta, 0 - \sin \theta, 0), \\ \varepsilon^2 &= (0, 1, 0, 0), \\ \varepsilon^3 &= (\gamma_\phi \sin \theta, 0, \gamma_\phi \cos \theta, \gamma_\phi v_\phi),\end{aligned}\quad (\text{A14})$$

where  $\gamma_\phi = E_\phi/M_\phi$ ,  $v_\phi = |\mathbf{q}|/E_\phi$ . Using the polarization vectors in the helicity basis

$$\varepsilon^{*0} = \varepsilon^3, \quad \varepsilon^{*\pm 1} = \mp \frac{1}{\sqrt{2}}(\varepsilon^1 \mp i\varepsilon^2) \quad (\text{A15})$$

we get the amplitude in the  $\phi$  helicity basis as

$$W^0 = W^3, \quad W^{\pm 1} = \mp \frac{1}{\sqrt{2}}(W^1 \mp iW^2), \quad (\text{A16})$$

which may be directly used in numerical calculations.

---

[1] A.A. Sibirtsev, Nucl. Phys. A **604**, 455 (1996).

[2] W.S. Chung, G.Q. Li, C.M. Ko, Phys. Lett. B **401**, 1 (1997); Nucl. Phys. A **625**, 347 (1997).

[3] F. Klingl, T. Wass, W. Weise, Phys. Lett. B **431**, 254 (1998).

[4] E.E. Kolomeitsev, D.N. Voskresensky, B. Kämpfer, Nucl. Phys. A **588**, 889 (1995).

[5] R. Barth et al. (KAOS collaboration), Phys. Rev. Lett. **78**, 4007 (1997).

[6] N. Herrmann (FOPI collaboration), Nucl. Phys. A **610**, 49c (1996).

[7] J. Friese et al. (HADES collaboration), GSI report 97-1, p. 193 (1997)

[8] F. Balestra et al. (DISTO collaboration), Phys. Rev. Lett. in print

[9] M.G. Sapozhnikov et al., COSY Letter of Intent # 35 (1995);  
     C. Wilkin, internal report to the COSY ZDF group (unpublished).

[10] J. Ellis, M. Karliner, D.E. Kharzeev, M.G. Sapozhnikov, Phys. Lett. B **353**, 319 (1995).

[11] M.P. Locher, Y. Lu, Z. Phys. A **351**, 83 (1995);  
     D. Buzatu, F. M. Lev, Phys. Lett. B **329**, 143 (1994).

[12] J. Gasser, H. Leutwyler, M.E. Sainio, Phys. Lett. B **253**, 252 (1991).

[13] D.B. Kaplan, A.V. Manohar, Nucl. Phys. B **310** 527 (1988);  
     R.D. McKeown, Phys. Lett. B **219**, 140 (1989);  
     E.M. Henley, G. Krein, S.J. Pollock, A.G. Williams, Phys. Lett. B **269**, 31 (1991).

[14] A.I. Titov, Y. Oh, S.N. Yang, Phys. Rev. Lett. **79**, 1634 (1997); Nucl. Phys. A **618**, 259 (1997).

[15] M.P. Rekalo, J. Arvieux, E. Tomasi-Gustafsson, Z. Phys. A **357**, 133 (1997).

[16] A. Engel, R. Shyam, U. Mosel, A.K. Dutt-Mazumder, Nucl. Phys. A **603**, 387 (1996);  
     V. Shklyar, B. Kämpfer, B.L. Reznik, A.I. Titov, Nucl. Phys. A **628**, 255 (1998).

[17] E.M. Henley, G. Krein, A.G. Williams, Phys. Lett. B **281**, 178 (1992).

[18] M. Schäfer, H.C. Dönges, A. Engel, U. Mosel, Nucl. Phys. A **575**, 429 (1994).

[19] A.I. Titov, B. Kämpfer, E. Bratkovskaya, Phys. Rev. C **51**, 227 (1995).

[20] U.-G. Meissner, V. Mull, J. Speth, J.W. Van Orden, Phys. Lett. B **408**, 381 (1997).

[21] R.L. Jaffe, H. Lipkin, Phys. Lett. B **266**, 458 (1991);  
     J. Kepller, H.M. Hofmann, Phys. Rev. D **51**, 3936 (1995).

[22] W. Koepf, E.M. Henley, S.J. Pollock, Phys. Lett. B **288**, 11 (1992).

[23] B.L. Ioffe, M. Karliner, Phys. Lett. B **247**, 387 (1990).

[24] R. Machleidt, Adv. Nucl. Phys. **19**, 189 (1989).

[25] V. Flaminio, CERN preprint CERN-HERA 01/84 (1984).

[26] B. Friman, M. Soyer, Nucl. Phys. A **600**, 477 (1996).

[27] R. Baldi *et al.*, Phys. Lett. B **68**, 381 (1977); V. Blobel *et al.*, Phys. Lett. B **59**, 88 (1975).

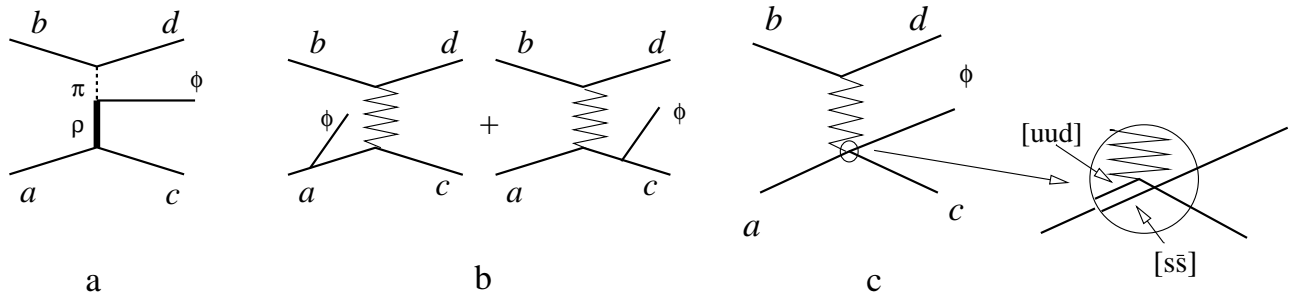


FIG. 1. Diagrammatic representation of processes of the  $\phi$  production: emission from (a) the internal meson line, (b) the external nucleon legs, and (c) the exchanged meson - nucleon vertex. Exchange diagrams are not displayed.

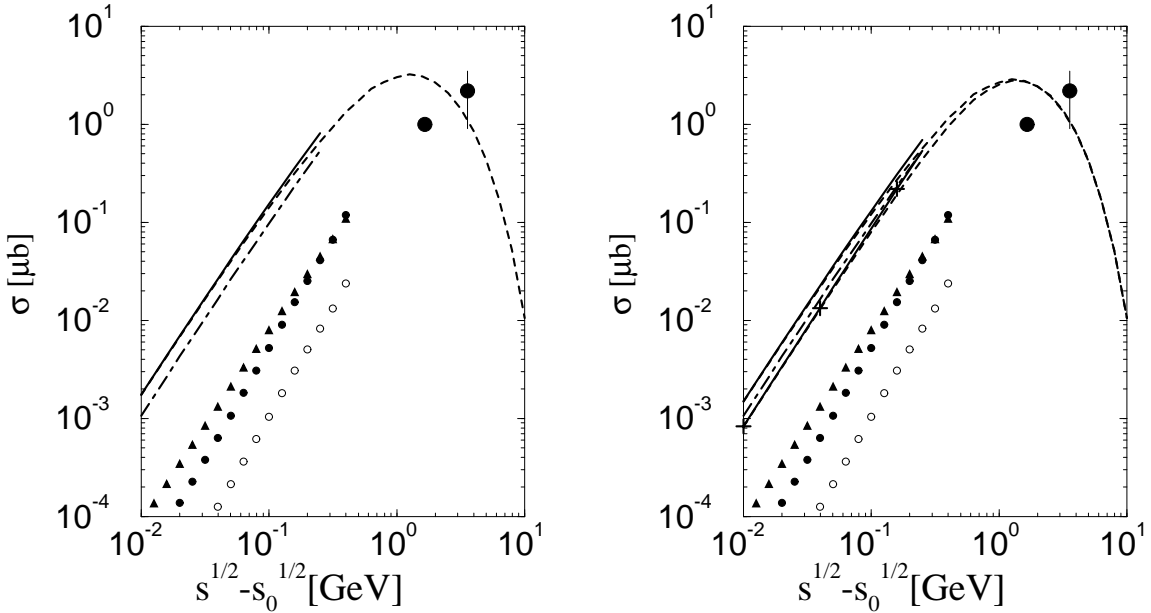


FIG. 2. The total cross section of the  $pp \rightarrow pp\phi$  reaction as a function of the excess energy. Data (fat dots) from [27]. The individual contributions are shown separately: pure OBE process 1a (dot-dashed lines),  $\phi$  bremsstrahlung 1b (triangles),  $\phi$  shake-off (open and filled circles for  $B^2 = 1$  and 5%). Solids lines depict the coherent sum of all amplitudes (with  $B^2=0.05$ ), while dashed lines represent these sums with additional energy depending effective cut-off described in text. Left panel: real two-body  $T$  (the difference between positive and negative values  $a_1$  is not seen on this scale); right panel: purely imaginary two-body  $T$  matrix (crosses mark the coherent sum with positive value of  $a_1$ ).

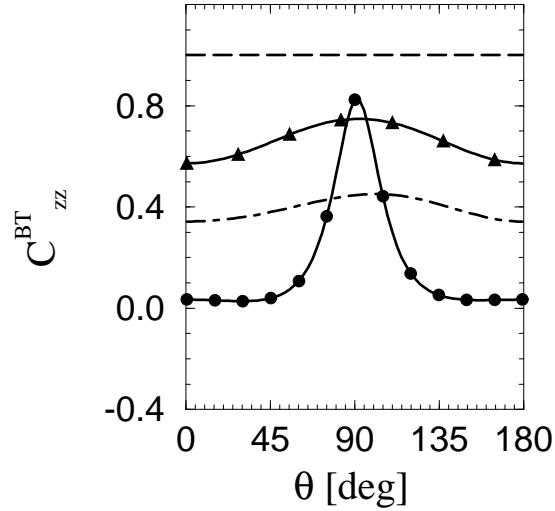


FIG. 3. The finite - energy beam-target asymmetry for the  $pp \rightarrow pp\phi$  reaction as a function of the c.m.s.  $\phi$  production angle  $\theta$  for different channels. The contribution from the OBE channel 1a is the dot-dashed line, the  $\phi$  bremsstrahlung channel 1b is marked by triangles, and the  $\phi$  shake-off 1c is marked by dots. The threshold prediction is depicted by the long-dashed line.

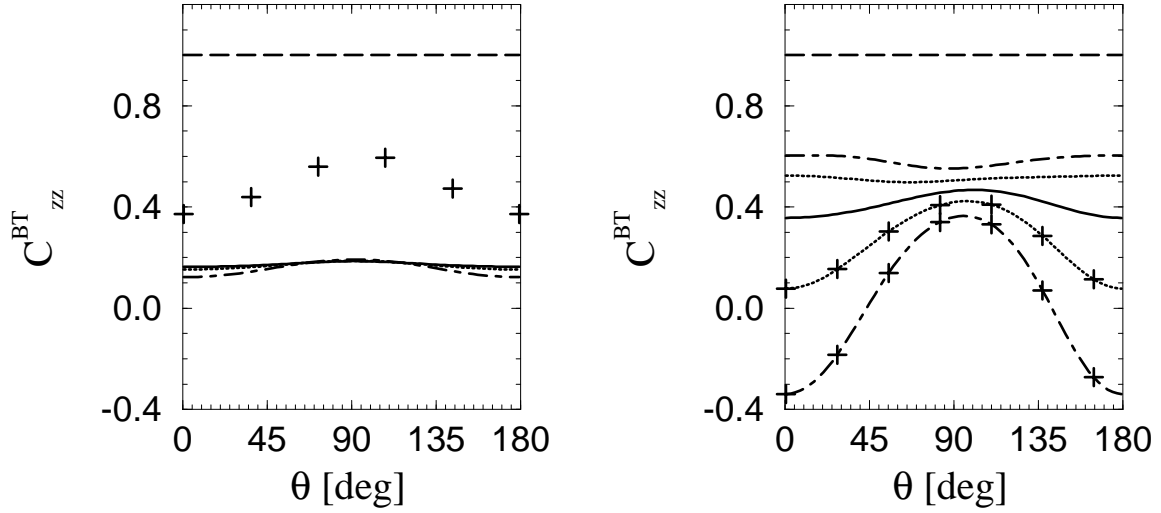


FIG. 4. The beam-target asymmetry as a coherent sum of all channels. Solid, dotted and dot-dashed lines correspond to  $B^2=0.$ ,  $0.01$  and  $0.05$ , respectively. Left panel: real two-body  $T$  matrix (the difference between positive and negative  $a_1$  values is not visible on this scale; crosses indicate the result for  $g_{\phi NN} = +0.24$ ); right panel: imaginary two-body  $T$  matrix (a positive value of  $a_1$  is marked by crosses). The threshold prediction is depicted by the long-dashed line.

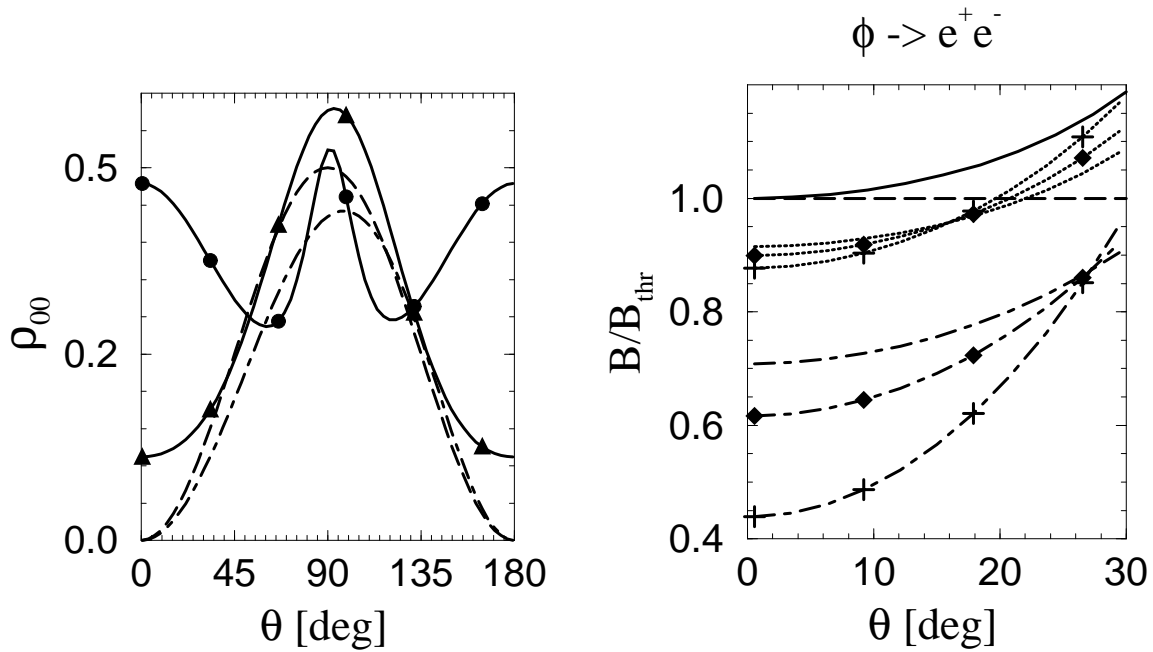


FIG. 5. The spin density matrix element  $\rho_{00}$  separately for different channels (left panel; notation as in Fig. 3) and the asymmetry of  $\phi \rightarrow e^+ e^-$  decays normalized to the threshold value (right panel; for an imaginary two body  $T$  matrix; notation as in right panel of Fig. 4; the results for a real phase are marked by diamonds).